The mass load effect on the resonant acoustic frequencies of colloidal semiconductor nanoplatelets

Adrien Girard, Lucien Saviot, Silvia Pedetti, Mickaël Tessier, Jérémie Margueritat, Hélène Gehan, Benoit Mahler, Benoit Dubertret, Alain Mermet

Journal Name

ARTICLE TYPE

Cite this: DOI: 10.1039/xxxxxxxxxx

Mass load effect on the resonant acoustic frequencies of colloidal semiconductor nanoplatelets

Adrien Girard,[a] Lucien Saviot,[b] Silvia Pedetti,[c] Mickaël D. Tessier,[c] Jérémie Margueritat,[a] Hélène Gehan,[a] Benoit Mahler,[a] Benoit Dubertret,[c] and Alain Mermet*[a]

Received Date
Accepted Date

DOI: 10.1039/xxxxxxxxxx

www.rsc.org/journalname

Resonant acoustic modes of ultrathin CdS and CdSe colloidal nanoplatelets (NPLs) with varying thicknesses were probed using low frequency Raman scattering. The spectra are dominated by an intense band ascribed to the thickness breathing mode of the 2D nanostructures. The measured Raman frequencies show strong deviations with respect to values expected for simple bare plates, all the more so as the thickness is reduced. The deviation is shown to arise from the additional mass of the organic ligands that are bound to the free surfaces of the nanoplatelets. Calculating the eigenfrequencies of vibrating platelets weighted down by the mass of the organic ligands provides very good agreement with the observed experimental behaviours. This finding opens up a new possibility of nanomechanical sensing such as nanobalances.

Resonant acoustic modes are typical manifestations of size effects that occur as the wavelength of the vibration approaches the size of the system that sustains it. Macroscopic examples of resonant acoustic modes are 1D standing waves of a string, 2D flexural modes of plates or 3D breathing-like oscillations of spheres. Nowadays, the nanoscale equivalent of these types of modes raises strong interest particularly for nanoelectromechanical system (NEMS) applications. The most common way of exploiting nanomechanical modes for sensing purposes is to resonantly excite them through electrical actuators and track resonance frequency changes due to external perturbations (mass loading, pressure, deformation...). The typical frequencies of the so-solicited mechanical resonances lie in the sub-GHz or GHz range and the mode shapes can cover a wide variety of displacement fields (bending motion of a cantilever or of a long nanotube[1], flexural modes of nanosheets[2],...). A key challenge in NEMS applications is to develop smaller and lighter resonators operating at higher frequencies with good quality factors. Since resonance frequencies scale with inverse sizes, nano-objects with very small dimensions (of a few nanometers) potentially fulfill these requirements; yet, detecting their very high resonance frequencies approaching the THz range require different experimental setups than the classical electromechanical devices.

Inelastic Raman light scattering at low frequencies has proved as an efficient tool to probe resonant acoustic mode frequencies of nano-objects with very small sizes. Initially developed from quasi-spherical nanocrystals nucleated in glasses[3], this technique has been successfully employed to characterize resonant acoustic modes (also called Lamb modes) from a variety of spherical nanostructures like quantum dots[4,5], metallic nanospheres[6–8] or dielectric nanoparticles[9–11].

Compared to spherical or quasi-spherical nanostructures, investigations of resonant acoustic modes from 2D nano-objects with nanometer thicknesses are more scarce. Recent low frequency Raman works on a few layer graphene sheets[12] identified interlayer shear modes below 50 cm^{-1} (1.5 THz) thus enabling to probe the interlayer interactions. Similar measurements on nanosheets of transition metal dichalcogenides[13] also led to the detection of interlayer shear modes together with a new type of mode ascribed to the breathing thickness vibration of the nanosheets. This latter mode is the 2D equivalent of the spherically symetrical breathing vibration of a nanosphere (also referred to as the $\ell = 0$ Lamb mode) that is routinely detected in low frequency Raman spectra from spherical nanoparticles[14]. Like for spherical nanoparticles, the experimental Raman breathing mode frequencies of the 2D nanosheets were found to well agree with the values derived from the continuum elasticity approach whereby the nanosheet is modeled as a freely vibrating plate.

The present paper is dedicated to the low frequency Raman

[a] *Institut Lumière Matière, Université de Lyon, Université Claude Bernard Lyon 1, UMR CNRS 5306, 69622 Villeurbanne, France*
[b] *Laboratoire Interdisciplinaire Carnot de Bourgogne, UMR 6303 CNRS-Université de Bourgogne Franche Comté, 9 Av. A. Savary, BP 47 870, F-21078 Dijon Cedex, France*
[c] *Laboratoire de Physique et d'Etudes des Matériaux, CNRS, Université Pierre et Marie Curie, ESPCI, 10 rue Vauquelin, 75005 Paris, France*
* alain.mermet@univ-lyon1.fr

characterization of the thickness breathing mode from atomically flat colloidal semi-conductor nanoplatelets. At variance with comparable measurements on the exfoliated nanosheet systems, strong deviations from freely vibrating plate frequencies are observed. We show that these deviations are caused by the additional mass load of the organic ligands lying at the surface of the nanoplatelets, differently from known acoustic impedance effects inherent of a continuous surrounding medium.

CdS and CdSe NPLs were synthesized through colloidal chemistry routes in the zinc-blende (ZB) structure[15,16]. NPLs with thickness ranging between 3 and 5 monolayers (MLs) were obtained using hot injection reactions previously described[17]. Sulfur and selenium precursors, respectively, were injected at high temperatures (between 180 and 250 °C) into a reaction mixture of cadmium carboxylate complexes in 1-octadecene. CdS and CdSe NPLs possessing thicknesses larger than 5 MLs were prepared through colloidal atomic layer deposition reactions (c-ALD[16]). This technique allows the deposition of several CdS and CdSe monolayers on thinner CdS and CdSe NPLs, respectively. The reaction is performed at room temperature using inorganic ions precursors dispersed in organic polar solvent such as N-methylformamide (NMF)[16]. The monolayers growth occurs by the alternate reaction of anionic and then cationic precursors at the large top and bottom lateral surfaces of thinner NPLs cores. For example, CdSe NPLs with 11 MLs were obtained growing four additional CdSe layers on CdSe NPLs with 3 MLs.

While the lateral dimensions of the NPLs (of the order of tens to a hundred nanometers) are difficult to control, their thicknesses can be precisely adjusted between 3 and 14 ML, *i.e.* between approximately 1 nm and 4 nm respectively[18]. The large bottom and top faces of the nanoplatelets are (100) faces bearing Cd^{+} cations that are bound to oleate (OA) ligands. Detailed morphological characterizations and thickness evaluations through transmission electron microscopy and high-angle annular dark field TEM are given elsewhere[16,18].

UV-visible absorption spectra of the NPLs dissolved in their native solvents (hexane or toluene) are displayed in Figure 1(A),(C). These spectra show remarkably narrow absorption bands associated with the strong confinement of the exciton across the NPL thicknesses and with a negligible dependence on their lateral dimensions[19]. The sharpness of the excitonic transitions, relative to the heavy hole- and light hole- to electron transitions (hh-e and lh-e), reflects the high thickness monodispersity of the NPL assemblies which is a definite asset for the low frequency Raman characterizations. While the heavy hole absorption edge in CdSe NPLs shifts from 450 nm up to 650 nm as thicknesses increase from 3 ML up to 11 ML respectively, in CdS it only shifts from 405 nm up to 500 nm over the 4 - 14 ML thickness range.

The Raman measurements were performed from evaporated drops of solutions on copper substrates at room temperature. The Raman frequencies were determined from measurements with different spectrometers operating either at fixed (532 nm and 633 nm) or adjustable (660 nm, 560 nm, 514.5 nm and 496.5 nm) excitation wavelengths in order to work in nearly resonant conditions with the hh exciton (see Supplementary Information). Double checking the Raman frequency values with different excitation wavelengths did not reveal any significant resonance dependence, i.e. frequency values agreed within ±5% whatever the excitation wavelength.

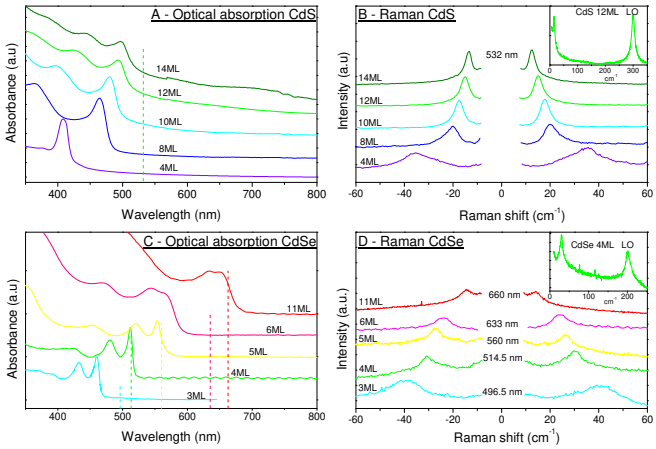

Fig. 1 *Top graphs*: Optical absorption spectra of CdS (A) and CdSe (C) NPLs nanoplatelets with varying thicknesses (ML=monolayer). Dashed vertical lines indicate the Raman excitation wavelengths. *Bottom graphs*: corresponding low frequency Raman spectra of CdS (B) and CdSe (D) NPLs. For CdSe NPLs the different Raman excitation lines are indicated.

Figure 1(B) and (D) show the low frequency Raman spectra of the CdS and CdSe NPLs. For both systems, one observes a well defined Raman peak shifting from about 10 cm^{-1} up to about 35 cm^{-1} as the thickness of the NPLs decreases. This low frequency Raman signal can be safely associated with the NPLs as the larger range Raman spectra (insets of Figure 1(c),(d)) attest the detection of the longitudinal optical modes near 300 cm^{-1} and 200 cm^{-1} for CdS and CdSe NPLs respectively. The detailed study of the dependence of the LO modes upon the NPL thicknesses was reported previously[20,21]; it lies outside the scope of this paper.

Figure 2 reports the dependence of the low frequency mode versus the inverse thickness ($1/h$) of the nanoplatelets. At first order, the dependence is observed to be linear. Along similar inelastic light scattering experiments from thin films[22,23], the most natural explanation for this behavior is a 'thickness mode' which consists of a longitudinal standing wave across the thickness of the platelet. In the case of a freely vibrating plate the fundamental frequency of such mode depends on the elastic constant C_{11} and on the density ρ of the plate according to

$$\nu = \frac{1}{2h}\sqrt{\frac{C_{11}}{\rho}} \qquad (1)$$

where $\sqrt{\frac{C_{11}}{\rho}} = V_L$ is the longitudinal sound velocity along the (100) thickness direction of the NPL material. This expression is typically used to evaluate the resonance frequencies of piezoelectric microplates[24] (notwithstanding the change of C_{11} for C_{33} whenever the piezoelectric material structure is non-cubic). Note that the inverse thickness dependence of the low frequency Raman mode implies that its spectral width decreases with increasing thickness (considering a nearly identical thickness distribution), as is observed in Figure 1(c) and (d).

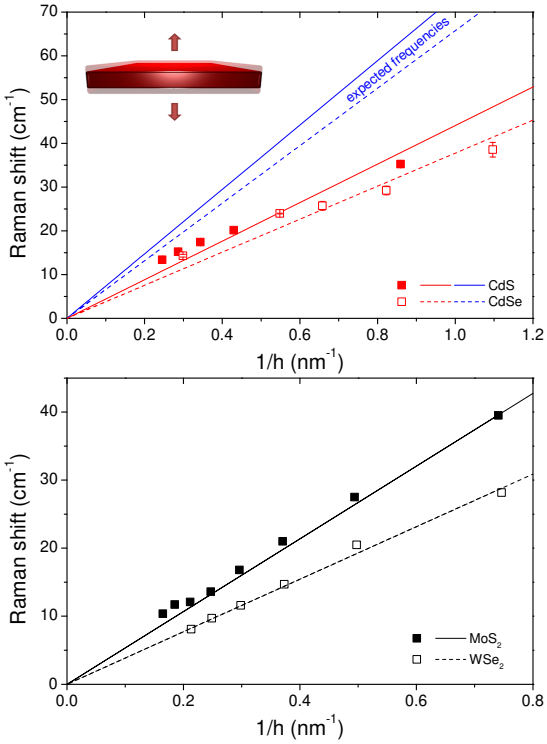

Fig. 2 *Top graph*: Evolution of the low frequency Raman shift with the inverse nanoplatelet thickness for CdS and CdSe NPLs (symbols). If not visible, error bars are within symbol sizes. Low slope lines are best linear fits to the data. Larger slope lines are calculated expected frequencies with corresponding bulk values of C_{11}^{ZB} and ρ_{ZB} of CdS and CdSe. *Bottom graph*: Experimental Raman shifts (symbols) and calculated expected frequencies with bulk C_{33} values for MoS_2 and WSe_2 exfoliated nanosheets from Ref. [13].

Linear fits with zero intercept over the full set of data (low slope lines in Figure 2) yield average values of $\langle C_{11}^{CdS} \rangle = 34 \pm 4$ GPa and $\langle C_{11}^{CdSe} \rangle = 29 \pm 2$ GPa, using the macroscopic mass densities $\rho_{ZB\text{-}CdS} = 4870$ kg.m^{-3} and $\rho_{ZB\text{-}CdSe} = 5655$ kg.m^{-3}. These values are nearly a factor 3 smaller than the only known macroscopic values $C_{11}^{w\text{-}CdS} = 90.7$ GPa and $C_{11}^{w\text{-}CdSe} = 74.6$ GPa that stand for the wurtzite phases. Indeed since the ZB structures are only stabilized at the nanoscale, very little is known about their elastic parameters. Theoretical estimates [25] have led to comparable yet slightly larger values of C_{11} in the ZB phase than in the wurtzite phase, i.e. $C_{11}^{ZB\text{-}CdS} = 97.8$ GPa and $C_{11}^{ZB\text{-}CdSe} = 88.1$ GPa. We have checked the validity of the CdS ZB value by measuring the breathing Lamb modes from bare (i.e. with no ligands) CdS quantum dots having the ZB structure (see Supplementary Information). The derived experimental value $C_{11}^{ZB\text{-}CdS} = 98 \pm 2$ GPa is in very good agreement with the theoretical estimate [25]. In the following, we adopt $C_{11}^{ZB\text{-}CdS} = 98$ GPa and $C_{11}^{ZB\text{-}CdSe} = 88$ GPa [25].

Comparing the experimental Raman frequencies (symbols in Figure 2) with those expected from Equation 1 using the macroscopic values of C_{11}^{ZB} (larger slope lines in Figure 2) reveals that the resonance frequencies strongly deviate from the nominal values, all the more so as the thickness of the NPLs is reduced. This behaviour strikingly constrasts with that observed from exfoliated MoS_2 and WSe_2 nanosheets [13] (bottom graph of Figure 2) for which the Raman frequencies conform with those expected from the corresponding macroscopic values C_{33} and ρ downto thicknesses of 1.3 nm (see Supplementary Information).

The observed deviations with respect to the nominal frequencies derived from the bulk sound velocities $\sqrt{\frac{C_{11}}{\rho}}$ show two important characteristics: the reduction is not constant with thickness and it is quite significant (it reaches about -50% for the thinnest platelets). This reduction cannot be explained by a possible relaxation of lattice parameters which was shown to amount to a few percents [26]. It can neither be explained by different boundary conditions of the thickness mode, namely the case of a fully supported nanoplatelet with the resting face fixed and the opposite one free. Indeed, in these latter conditions, the prefactor $1/2e$ in Equation 1 should be replaced by $1/4e$, leading to a constant frequency reduction of -50% whatever the NPL thickness. Finally, assuming the NPLs as fully embedded in an organic matrix of acoustic impedance Z_m ($Z_m = \rho^m V_L^m$) would result essentially in a damping, i.e. a broadening of the Raman peaks without significant frequency shifts, as observed with embedded CdS spherical nanoparticles [27].

The fact that the observed resonance frequencies are all the more downshifted as the thickness of the NPLs is reduced points to a typical lumped mass effect of a resonator under an additional mass load. In the present case of colloidal NPLs, the mass of the organic ligands covering the free surfaces of the platelets, which is not taken into account in Equation 1, is expected to play the role of an additional mass.

In order to verify this assumption, we can model a ligand capped NPL as a freely vibrating* slab of thickness h centered

* Since from TEM [28] and SAXS [29] characterizations most NPLs lie within stacks formed

at $z=0$ with two identical surface layers of surface mass densities σ at $z=\pm\frac{h}{2}$. Assuming a purely longitudinal motion, the equation of motion for an element of mass $\delta M=\sigma\delta S$ writes as:

$$\delta S C_{11}\frac{\partial u}{\partial z}\left(z=\frac{h}{2},t\right)=-\delta M\frac{\partial^2 u}{\partial t^2}\left(z=\frac{h}{2},t\right) \quad (2)$$

where the left-hand expression is the pressure force acting on δM. Searching for symmetric standing wave solutions (because the anti-symmetric ones are not Raman-active):

$$u(z,t)=A\sin\left(\frac{\omega}{V_L}z\right)\left[B\cos(\omega t)+C\sin(\omega t)\right] \quad (3)$$

and applying the previous boundary condition leads to the transcendental equation:

$$C_{11}\frac{\omega}{V_L}\cos\left(\frac{\omega}{V_L}\frac{h}{2}\right)=\sigma\omega^2\sin\left(\frac{\omega}{V_L}\frac{h}{2}\right) \quad (4)$$

which, since $\rho V_L^2=C_{11}$, can be written as:

$$\cos\left(\frac{\omega}{V_L}\frac{h}{2}\right)=\frac{\sigma\omega}{\rho V_L}\sin\left(\frac{\omega}{V_L}\frac{h}{2}\right) \quad (5)$$

where $\omega=2\pi\nu$. The fundamental thickness breathing mode frequency is given by the smallest solution of this equation, which can only be obtained numerically on the basis of the input parameters C_{11}^{ZB}, ρ_{ZB} and σ_{OA}. σ_{OA} can be estimated from the number density of OA ligands. Indeed, charge neutrality of the NPLs imposes that each surface Cd^+ cation binds to one oleic acid ($M_{OA}=282.46$ g.mol^{-1}) so that according to the nominal surface density of 2 Cd^+ per a^2 in (100) planes of the ZB structure†, $\sigma_{OA}=\frac{2}{a^2}\frac{M_{OA}}{N_A}$ (N_A Avogadro number), i.e. 5.9 OA/nm^2 and 5.4 OA/nm^2 for CdS and CdSe respectively.

Figure 3 compares the results of the calculations with the experimental frequencies. Considering the absence of any fit parameter, the agreement is remarkable both qualitatively and quantitatively thereby confirming the assumed mass effect. The agreement between the experimental data points and the calculations may be improved by adjusting the input parameters ρ_{ZB}, C_{11}^{ZB} and σ_{OA}. Since there is no analytical expression for the lumped mass frequencies, we have tested the separate influences of the three parameters for the CdS NPLs (see Supplementary Info). It comes out that a better agreement can be obtained by either increasing ρ_{ZB} or σ_{OA} by 30% or reducing C_{11}^{ZB} by 10% or by varying simultaneously the three parameters in lower ratios. A sole effect of a 30% larger mass density seems however unlikely as the relaxation of the lattice parameters in NPLs is not expected to exceed a few percents[26]. Conversely, a 10% reduction of the elastic constant C_{11}^{ZB} with respect to the assumed value of 88 GPa (estimated from ab-initio calculations[25]) appears more plausible considering the expected effects of size reduction on the elastic properties of nanoplates[30–32]. The fact that both CdS and CdSe NPLs have the

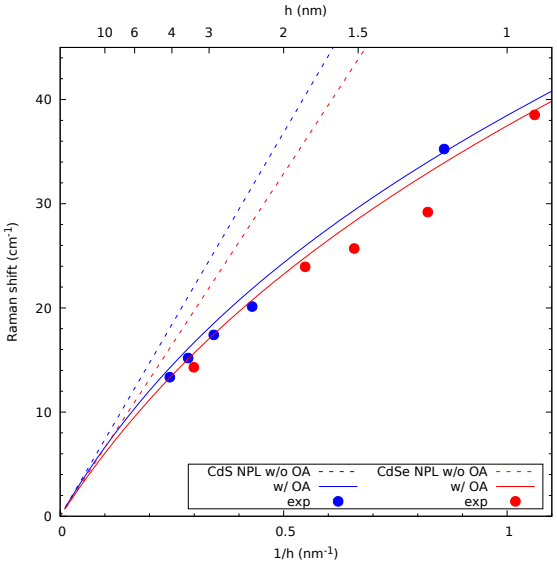

Fig. 3 Calculated thickness breathing mode frequencies (solid lines) of CdS and CdSe NPLs derived from a mass sandwich nanoplate model assuming a stoechiometric Cd^+/OA^- 1:1 ratio for the ligand surface mass densities σ_{OA}. Symbols are experimental frequencies and dashed lines are expected frequencies for bare NPLs.

tendency to curl at very small thicknesses[29,33] is indeed an indication of perturbed elasticity. Finally, the range of acceptable adjustability for σ_{OA} remains to be better characterized. Comparing the assumed OA number density of 5.4 OA/nm^2 for CdSe NPLs with that of 4.6 OA/nm^2 measured through NMR spectrometry from CdSe quantum dots capped with OA ligands[34] points to an already large value. Yet, the smaller value observed in QDs can be explained by the fact that the different facets of QDs are not all (100) planes resulting in a lower average Cd^+ density compared to NPLs. It therefore appears inappropriate to increase σ_{OA} to obtain a better agreement between the experimental and the calculated frequencies. Note that the purification steps during the synthesis of the NPLs may lead to localized removals of the ligands or to extra mass loads from adsorbed reaction by-products. This might explain the relative data dispersion for CdSe NPLs; more systematic studies using fresh samples and different ligands can help clarify this situation.

From the above considerations, it occurs that the colloidal shell of a nano-object can significantly affect its vibration resonance frequency. Such finding contrasts with the widely studied cases of ligand capped metallic nanospheres (e.g. thiol capped Au[8] or Ag[6] nanoparticles) for which Lamb mode frequencies evaluated on the basis of freely vibrating bare nanospheres were found to agree well with the Raman experimental values. Considering that the surface-to-volume ratios of a nanosphere of radius r and of a nanoplatelet of thickness h are comparable ($3/r$ *vs* $2/h$ respectively), what appears as a decisive factor in the observation of the mass effect is the ratio of the soft shell surface mass density σ_{lig} to the hard core mass $\rho_{core}L$ (where L is the confining dimension of the nano-object, i.e. h or r): the lower $\sigma_{lig}/\rho_{core}L$, the weaker the effect on the resonance frequency. As an example, this ratio decreases by about a factor 5 going from an oleic acid capped CdS

thanks to slightly interdigitized ligands, the most natural boundary conditions to apply for an average NPL is free motions at both ends

† where a is the lattice parameter of the ZB structures, i.e. $a=0.582$ nm for CdS and $a=0.608$ nm for CdSe

NPL of 1 nm thickness to a dodecanethiol capped Au nanosphere of 3 nm diameter (assuming equal ligand surface number densities for NPLs and nanospheres). Our finding suggests that previous interpretations of significantly downshifted Lamb mode frequencies from very small ($r < 2$ nm) CdSe nanoparticles capped with comparable organic ligands[35] may have omitted this effect.

The evidencing of a lumped mass effect in the resonance frequencies of NPLs brings new insight into the effect of a surrounding on the vibration of nano-objects. So far, the effect of a surrounding on the Lamb modes of nanoparticles has been essentially described by acoustic mismatch effects that have proved well suited for nanoparticles embedded in a matrix[36,37]. The impact of an embedding medium on the resonance frequencies of nanospheres can be estimated thanks to the Complex Frequency Method[27]; it essentially consists in a broadening of the Raman peaks. The presently evidenced mass effect differs from this approach in the sense that the close environment of the nano-object behaves more as an additional inert load rather than as a continuous medium with an acoustic impedance. This implies that at the probed frequencies the dynamics of the ligands is closer to single particle dynamics rather than to phonon-like collective dynamics. This novel ingredient of core-shell nano-object vibrations deserves better characterization.

As a conclusion, the thickness breathing modes of CdS and CdSe colloidal nanoplatelets with thicknesses varying between 1 and 4 nm were probed thanks to low frequency Raman scattering. Unlike similarly investigated systems (nanospheres or exfoliated nanosheets), the resonance frequencies were found to be strongly downshifted with respect to the expected frequencies of freely vibrating plates. Taking into account a lumped mass effect due to the presence of organic ligands at the surface of the nanoplatelets proves to well describe the deviation. The strong reduction (reaching nearly 50%) of the resonance frequencies observed for the thinnest nanoplatelets allows to envisage their use as molecular mass sensors. Compared to other nano-objects like binanopyramids[38], the nanobalance effect using nanoplatelets is expected to be much more sensitive thanks to their extended lateral faces combined very small thicknesses.

These works were supported by the ANR Nanovip project, grant ANR-13-JS10-0002 of the French Agence Nationale de la Recherche.

References

1 J. Chaste, A. Eichler, J. Moser, G. Ceballos, R. Rurali and B. A., *Nat Nano*, 2012, **7**, 301–304.

2 C. Chen, S. Rosenblatt, K. I. Bolotin, W. Kalb, P. Kim, I. Kymissis, H. L. Stormer, T. F. Heinz and J. Hone, *Nat Nano*, 2009, **4**, 861–867.

3 E. Duval, A. Boukenter and B. Champagnon, *Phys. Rev. Lett.*, 1986, **56**, 2052–2055.

4 L. Saviot, B. Champagnon, E. Duval, I. A. Kudriavtsev and A. I. Ekimov, *Journal of Non-Crystalline Solids*, 1996, **197**, 238–246.

5 M. Ivanda, K. Babocsi, C. Dem, M. Schmitt, M. Montagna and W. Kiefer, *Physical Review B*, 2003, **67**, 235329.

6 A. Courty, A. Mermet, P. A. Albouy, E. Duval and M. P. Pileni, *Nature Materials*, 2005, **4**, 395–398.

7 B. Palpant, H. Portales, L. Saviot, J. Lerme, B. Prevel, M. Pellarin, E. Duval, A. Perez and M. Broyer, *Phys. Rev. B*, 1999, **60**, 17107–.

8 H. Portales, N. Goubet, L. Saviot, S. Adichtchev, D. B. Murray, A. Mermet, E. Duval and M.-P. Pileni, *Proceedings of the National Academy of Sciences*, 2008, **105**, 14784–14789.

9 C. Pighini, D. Aymes, N. Millot and L. Saviot, *Journal of Nanoparticle Research*, 2007, **9**, 309–315.

10 L. Saviot, D. Machon, A. Mermet, D. B. Murray, S. Adichtchev, J. Margueritat, F. Demoisson, M. Ariane and M. d. C. Marco de Lucas, *J. Phys. Chem. C*, 2012, **116**, 22043–22050.

11 M. Mattarelli, M. Montagna, F. Rossi, A. Chiasera and M. Ferrari, *Phys. Rev. B*, 2006, **74**, 153412.

12 P. H. Tan, W. P. Han, W. J. Zhao, Z. H. Wu, K. Chang, H. Wang, Y. F. Wang, N. Bonini, N. Marzari, N. Pugno, G. Savini, A. Lombardo and A. C. Ferrari, *Nature materials*, 2012, **11**, 294–300.

13 Y. Zhao, X. Luo, H. Li, J. Zhang, P. T. Araujo, C. K. Gan, J. Wu, H. Zhang, S. Y. Quek, M. S. Dresselhaus and Q. Xiong, *Nano Letters*, 2013, **13**, 1007–1015.

14 L. Saviot, A. Mermet and E. Duval, in *Nanoparticles and Quantum Dots*, ed. K. D. Sattler, CRC Press, 2010, ch. 11, pp. 11.1–11.17.

15 S. Ithurria and B. Dubertret, *Journal of the American Chemical Society*, 2008, **130**, 16504–5.

16 S. Ithurria and D. V. Talapin, *Journal of the American Chemical Society*, 2012, **134**, 18585–90.

17 S. Ithurria, M. D. Tessier, B. Mahler, R. P. S. M. Lobo, B. Dubertret and A. L. Efros, *Nature Materials*, 2011, **10**, 936–941.

18 B. Mahler, B. Nadal, C. Bouet, G. Patriarche and B. Dubertret, *Journal of the American Chemical Society*, 2012, **134**, 18591–8.

19 S. Ithurria, G. Bousquet and B. Dubertret, *Journal of the American Chemical Society*, 2011, **133**, 3070–3077.

20 S. A. Cherevkov, A. V. Fedorov, M. V. Artemyev, A. V. Prudnikau and A. V. Baranov, *Phys. Rev. B*, 2013, **88**, 041303.

21 D. O. Sigle, J. T. Hugall, S. Ithurria, B. Dubertret and J. J. Baumberg, *Physical Review Letters*, 2014, **113**, 087402.

22 J. Groenen, F. Poinsotte, A. Zwick, C. M. Sotomayor Torres, M. Prunnila and J. Ahopelto, *Phys. Rev. B*, 2008, **77**, 045420.

23 N. Gomopoulos, W. Cheng, M. Efremov, P. F. Nealey and G. Fytas, *Macromolecules*, 2009, **42**, 7164–7167.

24 S. Fujishima, *CRC handbook of electrical filters*, Boca Raton: CRC Press., 1997.

25 E. Deligoz, K. Colakoglu and Y. Ciftci, *Physica B: Condensed Matter*, 2006, **373**, 124–130.

26 D. Chen, Y. Gao, Y. Chen, Y. Ren and X. Peng, *Nano Letters*, 2015, **15**, 4477–4482.

27 D. B. Murray and L. Saviot, *Phys. Rev. B*, 2004, **69**, 094305–9.

28 M. D. Tessier, L. Biadala, C. Bouet, S. Ithurria, B. Abecassis and B. Dubertret, *ACS Nano*, 2013, **7**, 3332–3340.

29 C. Bouet, B. Mahler, B. Nadal, B. Abecassis, M. D. Tessier, S. Ithurria, X. Xu and B. Dubertret, *Chemistry of Materials*, 2013, **25**, 639–645.

30 R. Dingreville and J. Qu, *Journal of the Mechanics and Physics of Solids*, 2005, **53**, 1827–1854.

31 L. G. Zhou and H. Huang, *Applied Physics Letters*, 2004, **84**, 1940.

32 R. E. Miller and V. B. Shenoy, *Nanotechnology*, 2000, **11**, 139.

33 E. M. Hutter, E. Bladt, B. Goris, F. Pietra, J. C. van der Bok, M. P. Boneschanscher, C. de Mello Donega, S. Bals and D. Vanmaekelbergh, *Nano Letters*, 2014, **14**, 6257–6262.

34 B. Fritzinger, R. K. Capek, K. Lambert, J. C. Martins and Z. Hens, *Journal of the American Chemical Society*, 2010, **132**, 10195–10201.

35 V. M. Huxter, A. Lee, S. S. Lo and G. D. Scholes, *Nano Letters*, 2009, **9**, 405–409.

36 S. Adichtchev, S. Sirotkin, G. Bachelier, L. Saviot, S. Etienne, B. Stephanidis, E. Duval and A. Mermet, *Phys. Rev. B*, 2009, **79**, 201402–4.

37 L. Saviot, D. B. Murray, E. Duval, A. Mermet, S. Sirotkin and M. d. C. Marco de Lucas, *Phys. Rev. B*, 2010, **82**, 115450–.

38 B. D. Fernandes, M. Spuch-Calvar, H. Baida, M. Treguer-Delapierre, J. OberlÃĨ, P. Langot and J. Burgin, *ACS Nano*, 2013, **7**, 7630–7639.

Journal Name

ARTICLE TYPE

Cite this: DOI: 10.1039/xxxxxxxxxx

Mass load effect on the the resonant acoustic frequencies of colloidal semiconductor nanoplatelets: Supplementary Information

Adrien Girard,[a] Lucien Saviot,[b] Silvia Pedetti,[c] Mickaël D. Tessier,[c] Jérémie Margueritat,[a] Hélène Gehan,[a] Benoit Mahler,[a] Benoit Dubertret,[c] and Alain Mermet*[a]

Received Date
Accepted Date

DOI: 10.1039/xxxxxxxxxx

www.rsc.org/journalname

1 Raman measurements from CdS and CdSe NPLs

In order to enhance the low frequency Raman signal, nearly resonant excitation conditions were chosen with Raman excitations lying slightly above the hh exciton absorption edge. This choice is a compromise to guarantee an enhanced interaction with light through strong absorption with a somewhat minimum photoluminescence which tends to dominate the Raman spectra and thus hide the weaker low frequency Raman signals. Because of the operation constraints of the Raman spectrometers, several setups were used.

A multichannel micro-Raman HORIBA Labram HR spectrometer equipped with Notch filters operating at the fixed excitation wavelength of 532 nm was used for all CdS samples. Differently, the strong shift of the NPL excitonic edge for CdSe samples required to operate with a wavelength versatile macro setup built of a 5-grating monochromator equipped with single channel detection. The Raman spectra of the 3 ML, 4 ML, 5 ML and 11 ML CdSe NPLs were recorded with the 496.5 nm, 514.5 nm, 560 nm and 660 nm excitation lines respectively. The 6 ML CdSe NPL sample was investigated with a Renishaw Invia micro-spectrometer operating at 633 nm.

For several samples, it was checked that the Raman frequencies did not depend significantly upon wavelength excitation (Figure 1). For CdSe NPLs, the frequencies were deduced from the average values between 532 nm and 633 nm.

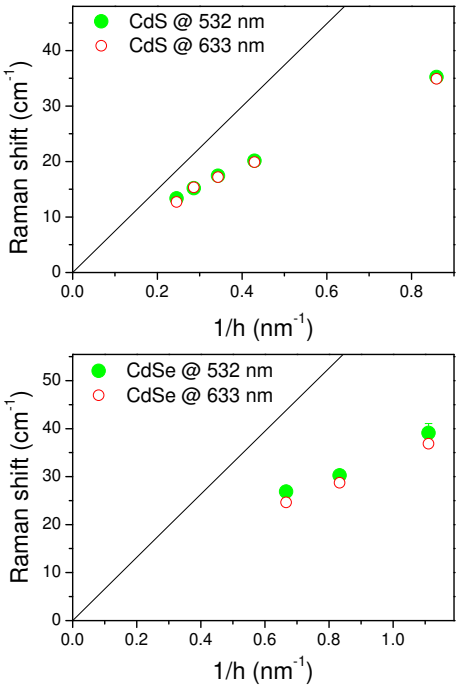

Fig. 1 Thickness mode frequency *vs* $1/h$ measured with 532 nm (full circles) and 633 nm (empty circles) excitation lines for selected CdS (top) and CdSe (bottom) NPL samples. No significant dependence upon wavelength excitation is observed. Lines are expected values from bare NPLs.

2 Determining C_{11} in Zinc-Blende CdS from quantum dots

Since bulk elastic constants of zinc-blende phase CdS and CdSe have, to our knowledge, not been characterized (available elastic data pertain essentially to the macroscopically stable wurtzite phase), we experimentally checked the value of $C_{11}^{ZB} = 98$ GPa

[a] *Institut Lumière Matière, Université de Lyon, Université Claude Bernard Lyon 1, UMR CNRS 5306, 69622 Villeurbanne, France*
[b] *Laboratoire Interdisciplinaire Carnot de Bourgogne, UMR 6303 CNRS-Université de Bourgogne Franche Comté, 9 Av. A. Savary, BP 47 870, F-21078 Dijon Cedex, France*
[c] *Laboratoire de Physique et d'Etudes des Matériaux, CNRS, Université Pierre et Marie Curie, ESPCI, 10 rue Vauquelin, 75005 Paris, France*
* alain.mermet@univ-lyon1.fr

which was derived from ab-initio calculations[1] for bulk ZB-CdS. To this end, bare (i.e. ligand free) CdS quantum dots in the ZB phase were synthesized in order to measure, through low frequency Raman scattering, one known Lamb mode whose frequency depend on the value of C_{11}^{ZB}.

2.1 Synthesis of the bare ZB-CdS QDs

10 mL 1-octadecene (ODE) and 800 μL Cd(oleate)$_2$ 0.5 M in oleic acid are introduced in a 100 mL three neck flask and degased for 30 min under vacuum at 70°C. Under Ar atmosphere, the temperature is raised to 250°C and 2 mL of S-ODE 0.1 M is swiftly injected. After 10 min annealing, half of the reaction mixture (5 mL) is taken out as sample 1. A stoichiometric mixture of S-ODE 0.1 M and Cd(oleate)$_2$ 0.5 M in oleic acid is then slowly injected (at 24 mL/h) and aliquots are taken at different times to obtain CdS nanocrystals samples of different sizes. The obtained nanocrystals samples have a mean sizes ranging from 4.8 nm to 7.2 nm diameter according to their absorption spectra[2] (Figure 2).

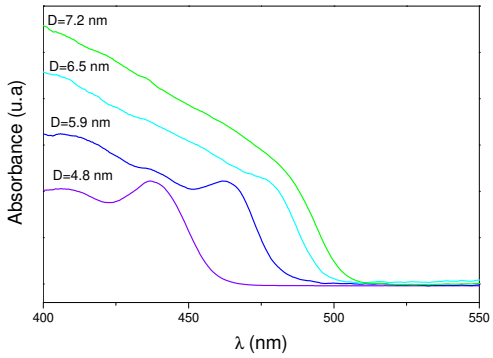

Fig. 2 Optical absorption spectra of bare ZB-CdS quantum dots with different diameters.

2.2 Raman measurements

The Raman measurements were performed in identical conditions as those described in the paper. Measurements were performed at 532 nm (using the HORIBA Labram HR micro-spectrometer) and at 633 nm (using the Renishaw Invia micro-spectrometer). Figure 3 displays the corresponding low frequency Raman spectra; once again, no dependence upon excitation wavelength is observed.

In accord with comparable measurements performed on CdS QDs embedded in glasses[3], the prominent peaks are ascribed to the fundamental breathing Lamb modes (described by the angular momentum $\ell = 0$) of the quasi-spherical QDs. For bare spherical nanoparticles, the Lamb $\ell = 0$ mode frequency is given by:

$$\nu_{\ell=0} \simeq 0.9\frac{V_L}{D} = \frac{0.9}{D}\sqrt{\frac{C_{11}}{\rho}} \quad (1)$$

A linear fit of the experimental frequencies (Figure 3- bottom) along this equation yields $C_{11}^{\text{ZB-CdS}} = 98$ GPa ($\rho_{\text{ZB-CdS}} = 4870$ kg.m^{-3}). This value is in excellent agreement with that derived from ab-initio calculations[1].

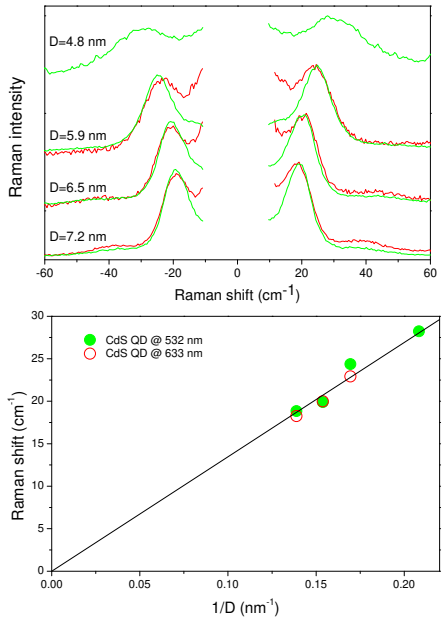

Fig. 3 Top : Low frequency Raman spectra of bare CdS quantum dots recorded with two different excitation wavelengths, 532 nm (green lines) and 633 nm (red lines). Indicated sizes are diameters. Bottom : Frequency dependence of reciprocal diameter $1/D$. The line is a zero intercept fit along Equation 1, yielding $C_{11}^{\text{CdS}} = 98 \pm 2$ GPa.

3 Analysis of published Raman data from MoS_2 and WSe_2 nanosheets[4]

Zhao *et al*[4] recently reported low frequency Raman measurements from MoS_2 and WSe_2 nanosheets with thicknesses lying between 1 and 6 nm. Compared to our colloidal NPLs, these systems have no ligands. Among the detected low frequency modes, two of them (named $B1$ and $B2$ in Ref.[4]) show frequencies decreasing with increasing thickness. DFT calculations[4] helped assign these modes to the fundamental and third overtone of so-called interlayer breathing modes. These modes are in fact thickness breathing modes, along the descriptions in Figure 4 of Ref.[4]. Accordingly, plotting the fundamental $B1$ frequencies of MoS_2 and WSe_2 nanosheets as a function of the corresponding reciprocal nanosheet thicknesses* (bottom graph of Figure 2 in the paper), one observes linear trends as expected from Equation 1 of the paper. Linear fits of these data yield, using macroscopic densities†, C_{33} values of 55 ± 2 GPa and 51 ± 1 GPa for MoS_2 and WSe_2 respectively (note that differently from cubic structures, the speed of sound in such hexagonal close packed structures along the thickness direction is given by $\sqrt{\frac{C_{33}}{\rho}}$). These values perfectly match the C_{33} values derived from the mass-spring model developed in Ref.[4].

* using 0.675 nm and 0.67 nm as one trilayer thickness in MoS_2 and WSe_2 respectively[5]

† *i.e.* 5.06 kg.m^{-3} and 9.32 kg.m^{-3} for MoS_2 and WSe_2 respectively

4 Evaluation of the influences of the parameters C_{11}, ρ and σ on the NPL frequencies

Figure 4 displays the separate dependencies of the lumped mass frequencies for CdS NPLs on the input parameters C_{11}, ρ and σ, i.e. changing one of the three parameters while fixing the two other ones at their nominal values ($C_{11}^{\text{ZB-CdS}} = 98$ GPa, $\rho_{\text{ZB-CdS}} = 4870$ kg.m^{-3} and $\sigma_{OA}^{CdS} = 5.9$ OA/nm^2). The results are commented in the main paper.

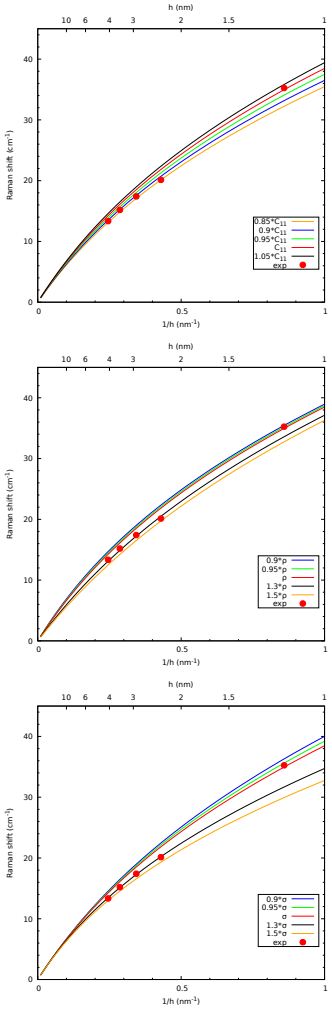

Fig. 4 Lumped mass frequencies for CdS NPLs changing C_{11} only (top), ρ only (middle) and σ only (bottom).

References

1 E. Deligoz, K. Colakoglu and Y. Ciftci, *Physica B: Condensed Matter*, 2006, **373**, 124–130.
2 W. W. Yu, L. Qu, W. Guo and X. Peng, *Chem. Mater.*, 2003, **15**, 2854–2860.
3 L. Saviot, B. Champagnon, E. Duval and A. I. Ekimov, *Phys. Rev. B*, 1998, **57**, 341–.
4 Y. Zhao, X. Luo, H. Li, J. Zhang, P. T. Araujo, C. K. Gan, J. Wu, H. Zhang, S. Y. Quek, M. S. Dresselhaus and Q. Xiong, *Nano Letters*, 2013, **13**, 1007–1015.
5 M. M. Benameur, B. Radisavljevic, J. S. Heron, S. Sahoo, H. Berger and A. Kis, *Nanotechnology*, 2011, **22**, 125706.